Niraparib Shows Superior Tissue Distribution and Efficacy in a Prostate Cancer Bone Metastasis Model Compared with Other PARP Inhibitors

Linda A. Snyder[1], Rajendra Damle[1], Shefali Patel[2], Jared Bohrer[2], Anna Fiorella[2], Jenny Driscoll[1], Rebecca Hawkins[1], Christopher F. Stratton[3], Carol D. Manning[1], Kanaka Tatikola[4], Volha Tryputsen[5], Kathryn Packman[6], and Rao N.V.S. Mamidi[7]

ABSTRACT

Patients with prostate cancer whose tumors bear deleterious mutations in DNA-repair pathways often respond to PARP inhibitors. Studies were conducted to compare the activity of several PARP inhibitors *in vitro* and their tissue exposure and *in vivo* efficacy in mice bearing PC-3M-luc-C6 prostate tumors grown subcutaneously or in bone. Niraparib, olaparib, rucaparib, and talazoparib were compared in proliferation assays, using several prostate tumor cell lines and in a cell-free PARP-trapping assay. PC-3M-luc-C6 cells were approximately 12- to 20-fold more sensitive to PARP inhibition than other prostate tumor lines, suggesting that these cells bear a DNA damage repair defect. The tissue exposure and efficacy of these PARP inhibitors were evaluated *in vivo* in PC-3M-luc-C6 subcutaneous and bone metastasis tumor models. A steady-state pharmacokinetic study in PC-3M-luc-C6 tumor-bearing mice showed that all of the PARP inhibitors had favorable subcutaneous tumor exposure, but niraparib was differentiated by superior bone marrow exposure compared with the other drugs. In a PC-3M-luc-C6 subcutaneous tumor efficacy study, niraparib, olaparib, and talazoparib inhibited tumor growth and increased survival to a similar degree. In contrast, in the PC-3M-luc-C6 bone metastasis model, niraparib showed the most potent inhibition of bone tumor growth compared with the other therapies (67% vs. 40%–45% on day 17), and the best survival improvement over vehicle control [hazard ratio (HR), 0.28 vs. HR, 0.46–0.59] and over other therapies (HR, 1.68–2.16). These results show that niraparib has superior bone marrow exposure and greater inhibition of tumor growth in bone, compared with olaparib, rucaparib, and talazoparib.

Introduction

It was estimated that more than 190,000 men were newly diagnosed with prostate cancer in the United States in 2020, making it the most common noncutaneous cancer in men and the third most common cancer overall (1). The androgen receptor signaling pathway is the main driver in the genesis and progression of this disease, in both the hormone-sensitive and castration-resistant phases (2). Recently, alterations in DNA-damage repair (DDR) pathways, such as in the genes for *BRCA1 DNA* repair-associated (*BRCA1*) and *BRCA2 DNA* repair-associated (*BRCA2*), have been identified in a substantial proportion of late-stage prostate tumors (3). Cells with defects in homologous recombination (such as *BRCA2* mutations) cannot tolerate simultaneous loss of PARP activity caused by PARP inhibition, and therefore undergo cell death due to synthetic lethality (4, 5). This observation has translated into successful clinical development of several PARP inhibitors in ovarian cancer (6–8), which has a high proportion of tumors with DDR defects (9). Results of clinical trials conducted in patients with prostate cancer show that niraparib, olaparib, and rucaparib are active against tumors deficient in DDR (10–14), offering a new treatment paradigm for this disease.

Prostate cancer frequently metastasizes to bone, resulting in bone pain, fractures, and spinal cord compression in late stages of disease (15). Tumor growth in bone marrow can lead to anemia and thrombocytopenia (16–18), which adversely affect the patient's quality of life. Results from nonclinical studies suggest that PARP inhibitors differ in their ability to penetrate bone marrow (19, 20), raising the possibility that PARP inhibitors might be differentiated by their antitumor activity toward tumors growing in bone. More specifically, PARP inhibitors vary in their permeability coefficients and solubility, likely affecting their activity *in vivo*: Niraparib has a higher apparent permeability coefficient (21), whereas olaparib, rucaparib, and talazoparib have low solubility in aqueous solution and moderate or low cell permeability (22–24). To evaluate these hypotheses, we compared niraparib, olaparib, rucaparib, and talazoparib in *in vitro* assays, and compared their tissue exposure and antitumor activity *in vivo* using prostate tumor models grown subcutaneously and in bone.

Materials and Methods

Reagents

Niraparib powder was supplied by Janssen Pharmaceuticals; olaparib, rucaparib, and talazoparib were obtained as powder from

[1]Oncology Discovery, Janssen Research and Development, Spring House, Pennsylvania. [2]Drug Metabolism and Pharmacokinetics, Janssen Research and Development, Spring House, Pennsylvania. [3]Discovery Sciences, Janssen Research and Development, Spring House, Pennsylvania. [4]Statistics and Decision Sciences, Janssen Research and Development, Raritan, New Jersey. [5]Statistics and Decision Sciences, Janssen Research and Development, Spring House, Pennsylvania. [6]Oncology *In Vivo* Pharmacology, Janssen Research and Development, Spring House, Pennsylvania. [7]Global Drug Metabolism and Pharmacokinetics, Janssen Research and Development, Raritan, New Jersey.

Note: Supplementary data for this article are available at Molecular Cancer Therapeutics Online (http://mct.aacrjournals.org/).

Current address for R. Damle: Parexel International, Newton, MA.

Corresponding Author: Linda A. Snyder, Janssen Research and Development, 1400 McKean Road, Spring House, PA 19477. Phone: 215-628-5178; Fax: 610-889-4623; E-mail: LSnyder2@its.jnj.com

Mol Cancer Ther 2022;21:1115–24

doi: 10.1158/1535-7163.MCT-21-0798

SelleckChem (catalog Nos. S1060, S1098, S7048, respectively). All were stored at −20°C, either as powder or dissolved in DMSO.

Cell lines and gene profiling

PC-3M-luc-C6 cells (RRID:CVCL_D577) were licensed from Covance (formerly MI Bioresearch). LNCaP (catalog No. CRL-1740, RRID:CVCL_1379) and DU145 cells (catalog No. HTB-81, RRID:CVCL_0105) were purchased from the ATCC. LNCaP-AR cells were licensed from Aragon Pharmaceuticals (25). Before use, all cell lines were determined to be free of *Mycoplasma* contamination, using MycoAlert *Mycoplasma* Detection Kit (Lonza catalog No. LT07-318). Cell lines were used for *in vitro* or *in vivo* experiments within 4 weeks of thaw. PC-3M-luc-C6 cells were grown in DMEM with GlutaMAX, 10% FBS, 1% nonessential amino acids (NEAAs); LNCaP and LNCaP-AR cells were grown in RPMI-1640 with GlutaMAX, 10% FBS, 1% NEAA; and DU145 cells were grown in Minimal Essential Medium with GlutaMAX, 10% FBS, 1% NEAA. All tissue culture reagents were purchased from Thermo Fisher Scientific. Each cell line was subjected to whole-exome sequencing and RNAseq (performed by Cofactor Genomics). Cell lines were analyzed for mutations in oncogenes and DDR pathway genes, including *PTEN*, *TP53*, *BRCA2*, *BRCA1*, and *ATM serine/threonine kinase*. DU145, LNCaP, and LNCaP-AR cell lines were authenticated by the Janssen cell bank using DNA fingerprinting.

In vitro proliferation assays

Cells were seeded in 96-well white flat-bottom tissue-culture plates at the appropriate density for a 6-day proliferation experiment, then incubated overnight at 37°C and 5% CO_2. The next day, PARP inhibitors were diluted to three times the final top concentration in medium, with a final DMSO concentration ≤1.5%. Working stocks were serially diluted into vehicle containing the same concentration of DMSO. Diluted PARP inhibitor, vehicle, or medium without DMSO was added to wells containing cells, with each condition tested in triplicate. Plates were incubated for 6 days at 37°C and 5% CO_2 and then assayed for viability using the CellTiter-Glo Luminescent Cell Viability Assay (Promega). Calculation of the percentage of inhibition was determined using the manufacturer's instructions and relative to the DMSO control.

DDR assay

Staining for phosphorylated histone H2A.X (γ-H2A.X) and RAD51 recombinase (RAD51) was used as a measure of DDR defects and was performed by Horizon Discovery Services. In brief, cells were seeded into 96-well optically clear plates and allowed to attach for 24 hours at 37°C and 5% CO_2 in a humidified environment. Niraparib was diluted in a semi log manner in DMSO and then in culture medium to generate a nine-point concentration-range from 10 μmol/L to 1 nmol/L. Etoposide was diluted in DMSO and then in culture medium for a final concentration of 3 μmol/L and served as a positive control for induction of DNA double-stranded breaks; medium containing 0.1% DMSO served as a negative control. All conditions were tested in triplicate. Cells were incubated for 18 hours with medium, niraparib or etoposide, fixed with 4% paraformaldehyde for 10 minutes at room temperature, washed once in PBS for 10 minutes, and permeabilized with PBS/0.1% Triton X-100 for 2 minutes. Cells were blocked with 10% goat serum (Cell Signaling Technology) in PBS/0.1% Triton X-100 for 1 hour and washed three times for 10 minutes per wash with PBS/Triton X-100 before incubation with RAD51 antibody (Abcam; catalog No. ab133534, RRID:AB_2722613; 1:500) and γ−H2A.X antibody (Millipore; catalog No. 05-636, RRID: AB_309864; 1:2,000) in PBS/0.1% Triton X-100 for 1 hour. Cells were washed three times for 10 minutes per wash and then incubated with goat anti-mouse IgG (H+L) cross-absorbed Alexa Fluor 488 (Thermo Fisher Scientific; A-11001, 1:500), goat anti-rabbit IgG (H+L) cross-absorbed Alexa Fluor 568 (Thermo Fisher Scientific; A-11036, 1:500)- and Hoechst dye (1 μg/mL) in PBS/0.1% Triton X-100 for 1 hour. Each plate was imaged using a ×20 and ×40 objective in an open aperture (widefield) mode on a high-content imager (IN Cell Analyzer 6000, GE Healthcare), with nine images acquired per well. Images recorded with the ×20 objective were analyzed using Cell Profiler software (version 2.2.0). Following image analysis, the mean foci count per nucleus and the percentage of cells positive for foci were plotted, using as cutoff values of >10 γ-H2A.X foci/nucleus or >5 RAD51 foci/nucleus.

Fluorescence polarization PARP-trapping assay

The PARPtrap Assay Kit (BPS Biosciences) was used to measure PARP/DNA complex formation. Assays were run per the manufacturer's instructions, but the assay format was reconfigured for 384-well plates with a final volume of 10 μL. The final concentration for compound titrations was 10 μmol/L–9 pmol/L, 1:4, 11 points, with the final point being DMSO control. Fluorescence polarization was read on a BMG PHERAstar FS multimode plate reader (BMG Labtech) using a 485/520/520 FP filter.

In vivo tumor models

In vivo studies were performed at Covance, using 5- to 7-week-old male athymic nude-*Foxn1*^{nu} mice (Envigo). Animal studies were conducted in compliance with the animal welfare guidelines of the National Institutes of Health, Janssen Pharmaceuticals, and with the approval of Covance's Animal Care and Use Committee. Niraparib and rucaparib were formulated in 0.5% (w/v) hydroxypropyl methylcellulose; olaparib was dissolved in DMSO at 50 mg/mL and then diluted 10-fold in 20% 2-hydroxypropyl-β-cyclodextrin; talazoparib was formulated in PEG400. The MTD levels for niraparib, olaparib, rucaparib, and talazoparib were determined for this mouse strain. On the basis of prior experience and published studies (20, 26, 27), niraparib, olaparib, and talazoparib were dosed orally once daily, whereas rucaparib was dosed orally every 12 hours, each in a volume of 10 mL/kg. Efficacy studies were performed using the PC-3M-luc-C6 subcutaneous or bone metastasis tumor models.

In vivo pharmacokinetics and efficacy in PC-3M-luc-C6 tumor models

For the subcutaneous efficacy model, mice were implanted with 5×10^6 tumor cells in the axilla. Mice were randomized into groups of 10 mice each, with a mean tumor volume of 140 mm^3. PARP inhibitors were administered orally at their MTD for 28 days (days 7–34). Tumor volume was calculated using the formula: tumor volume (mm^3) = $(D \times d^2)/2$, where "D" represents the larger diameter and "d" the smaller diameter of the tumor as determined by caliper measurements. Animals were removed from the study when either subcutaneous tumor volume (≥2,000 mm^3) or body weight loss ≥20% endpoints were reached.

A steady-state pharmacokinetic (PK) study was performed in male mice bearing PC-3M-luc-C6 subcutaneous tumors to compare tissue exposure profiles of the PARP inhibitors (for detailed study design, see Supplementary Fig. S1). Dosing was initiated once tumor volumes reached 200 to 300 mm^3 and proceeded for 5 days. Mice treated with niraparib, olaparib, or talazoparib were sampled starting just before the

fifth dose; mice treated with rucaparib were sampled just before the 10th dose. Subsequent sampling times varied depending on the expected half-life of each PARP inhibitor. At each time point, plasma, tumor, bone marrow, brain, and prostate were collected from three mice/group. Tissues and plasma were snap-frozen and stored at −80°C until analysis was performed.

Three independent studies were conducted for the bone metastasis model, and the results were pooled for a total of 39 to 41 mice/group. On day 0, 3×10^6 PC-3M-luc-C6 cells were implanted by intracardiac injection (ICI), and mice were imaged that day to verify successful injection. On day 3, mice were randomized into treatment groups to achieve the same mean body weight. PARP inhibitors were administered orally at their MTD for 35 days (days 3–37). To monitor tumor growth in bone, bioluminescence intensity (BLI) measurements were performed on the mandible and femurs of each mouse at several fixed timepoints (days 3, 7, 10, 14, and 17), several times during the remainder of the dosing period and at study termination on day 71. Individual mice were removed from the study based on body weight loss ≥20% or negative clinical signs and necropsied to confirm the presence of tumor.

PK sample analysis

PARP inhibitors were detected and quantified in plasma and tissues using LC-MS/MS. PBS was added to frozen tissue samples, followed by homogenization on wet ice using a Qiagen TissueRuptor.

Sample cleanup was performed using a protein precipitation method where calibration standards, quality controls, unknown samples, or blank matrix was aliquoted to a 2-mL 96-well plate. Then, 200 μL of internal standard working solution (500 ng/mL in acetonitrile) was added. The plate was vortex-mixed followed by centrifugation at 4,000 rpm for 10 minutes. After centrifugation, 50 μL of the supernatant were removed and aliquoted to a new 96-well plate, and 100 μL of deionized water was added to the supernatant. The resulting solution was vortex-mixed, and 5 μL of diluted sample was injected on an LC-MS/MS system.

Quantitative analysis for the PARP inhibitors was accomplished using a nonqualified LC-MS/MS assay, performed on a Shimadzu LC system with PAL autosampler, coupled to an AB SCIEX 4000 triple quadrupole mass spectrometer. A gradient elution was employed using 0.5% acetic acid in water as mobile phase A and methanol for mobile phase B. The initial gradient started at 20% B and held until 0.20 minutes. For the elution step, the %B gradually increased for 1.40 minutes, until 90% at 1.60 minutes. The gradient was held at 90% from 1.60 to 2.60 minutes for the wash period. (For niraparib, the gradient was held at 70% during the wash step instead of 90% for the same duration). Finally, the %B dropped from 90% (70% for niraparib) to 20% over 0.1 minutes, where it was held from 2.70 to 3.40 minutes for the equilibration step. A flow rate of 0.5 mL/min was maintained through a Phenomenex Luna Omega Polar C18 100Å column (2.1 × 50 mm, 5-μm particle size). Data were processed using Analyst 1.6.2 software. Chromatographic peaks for all four analytes and the internal standard were integrated using Analyst Intelliquan algorithm, and three peak smooths were used. Integration settings were applied globally to all samples.

Statistical analysis

In the proliferation assay comparing PARP inhibitors in the PC-3M-luc-C6 cells, nonlinear four-parameter logistic regression was performed on data from each compound. A global F test was performed on the top and bottom plateaus for each compound, which determined that the span of the percentage of inhibition was not significantly different across compounds. All pairwise comparisons of $\log EC_{50}$ estimates were performed, *P* values were reported, and $\log EC_{50}$ estimates and their 95% confidence intervals plotted to illustrate the results. No adjustments were made for multiple testing. The analysis was performed using GraphPad Prism version 9.0.0 for Windows (GraphPad Prism, RRID:SCR_002798). The figure illustrating *in vitro* niraparib cytotoxicity in four prostate tumor cell lines comprises results from two studies, and it was deemed inappropriate to compare the EC_{50} values statistically.

In vivo efficacy was evaluated both cross-sectionally and longitudinally. For cross-sectional evaluation, the percentage of tumor growth inhibition (% TGI) at a timepoint was defined as the difference between mean tumor volumes of the treated and control groups, calculated using the formula: $[(TV_c - TV_t)/TV_c] \times 100$, where TV_c is the mean tumor volume of the control group and TV_t is the mean tumor volume of the treatment group. The percentage of TGI was calculated for each of the treatment groups at day 23 (subcutaneous model) and day 17 (bone metastasis model) when at least 80% and 97% of mice per group, respectively, remained on study. For the subcutaneous and bone metastasis models, the percentage of TGI distribution was constructed by resampling animals 2,000 times with replacement (bootstrapping). For the subcutaneous model, at each sample, the observed number of animals was drawn from a respective treatment group, and the control group and the percentage of TGI was calculated. For the bone metastasis model, at each sample, the observed number of animals was drawn from a respective treatment group, and the control group; TV_c and TV_t were estimated using a linear mixed-effects (LME) model with a fixed effect for a treatment group and random effect for a study. %TGI was calculated using the LME-estimated treatment group means. For the subcutaneous and bone metastasis models, the 2.5% and 97.5% percentiles of the sampled %TGI distribution were taken as the lower and the upper bound of the % TGI 95% CI. The %TGI *P* value was calculated to test for the difference of the %TGI from zero and was constructed by investigating which quantile of the sampled %TGI distribution contained zero.

Longitudinal efficacy was evaluated through comparing treatment effect on change in tumor over time and was carried by fitting an LME model to log10-transformed tumor volume data. For the subcutaneous tumor model, LME with treatment and day of the study as fixed effects, and animal ID as random effect were fit to the tumor volume data. For the bone metastasis tumor model, the data up until day 31 of the study were considered to maintain sufficient sample size, and LME with treatment and day of the study as fixed effects, and animal ID and study number as random effects were fit to the tumor volume data. LME analyses were performed to compare the PARP inhibitors with the control and niraparib groups.

A Cox proportional hazards model was fit to the subcutaneous tumor model survival data to investigate association between the survival time and treatments. A Cox proportional hazards model with treatment-fixed effect and study random effect was fit to the bone metastasis data to evaluate differences in survival time between the treatment groups. The comparisons of interest were the PARP inhibitors compared with the control and niraparib treatment groups.

The percentage of increased lifespan (ILS) was calculated using the formula: [median survival time of the treatment group – median survival time of the control group)/median survival time of the control group] ×100.

For all tests, statistical significance cutoff value was set at alpha = 0.05.

PK data analysis

AUC estimation was achieved via noncompartmental theory. The concentrations are independent and identically distributed between animals. To approximate the concentration between the measured time points, the linear trapezoidal rule was used to find standard errors for AUCs. The individual contribution to the AUC of each animal was used, by finding the weighted sum of all measurements available for one animal where the weights corresponded to the weights from the trapezoidal rule. Taking the average of these individual contributions for all animals that have been undergoing the same sampling scheme gave the partial AUC. The standard error of the partial AUCs was found by using the sample standard deviation of the corresponding individual contributions. As the partial AUCs were independent of each other by construction, the standard error of the AUC was found by adding the standard errors of the partial AUCs.

For each PARP inhibitor and plasma/tissue, mean AUC for 24 hours (AUC_{0-24}) and the standard error are reported. Similarly, AUC_{0-24} tissue:plasma ratio and the corresponding standard error were calculated using the Fieller's theorem, which uses the standard errors of the AUCs and a critical value from a t-distribution with Satterthwaite's approximation to the degrees of freedom. R package "PK" was used to perform the analysis (28–30).

Data availability

All data are provided in the article and Supplementary Data Files.

Results

Impact of niraparib on proliferation of prostate tumor cell lines

Proliferation experiments were performed to assess the effect of niraparib on the growth of human prostate tumor cell lines (PC-3M-luc-C6, DU145, LNCaP, and LNCaP-AR) that differ in their oncogene and DDR gene profiles and Schlafen family member 11 expression (Supplementary Table S1).The IC_{50} value was 0.28 μmol/L for PC-3M-luc-C6 cells, 3.4 μmol/L for DU145 cells, 5.6 μmol/L for LNCaP cells, and 5.0 μmol/L for LNCaP-AR cells (**Fig. 1A**). The PC-3M-luc-C6 cells were 12- to 20-fold more sensitive to niraparib than the other cell lines, providing rationale for conducting *in vivo* efficacy studies using this model. This result suggested that the cells may have a defect in DDR, despite a lack of identified mutations in DDR genes as determined by whole-exome sequencing (Supplementary Table S1).

Assessment of DDR defect in PC-3M-luc-C6 cells

To investigate the impact of niraparib on the repair of DNA damage in PC-3M-luc-C6 cells, the cells were treated with a concentration-range of niraparib and then stained for γ-H2A.X and RAD51. H2A.X is recruited to sites of DNA double-stranded breaks to initiate repair; thus, increases in γ-H2A.X nuclear foci are an indicator of DNA damage (31). RAD51 plays an important role in repair and resolution of the lesions; therefore, increases in RAD51 foci correlate with repair (32). Treatment of PC-3M-luc-C6 cells with niraparib resulted in a concentration-dependent increase in DNA double-stranded breaks, as shown by increased numbers of γ-H2A.X foci per cell and the percentage of foci-positive cells (**Fig. 1B**). In contrast, the number of RAD51 foci kept pace with the number of γ-H2A.X foci per cell at lower drug concentrations, but the number of RAD51 foci leveled off and decreased at the higher concentrations of niraparib. This result provides additional support for the hypothesis that DDR is somewhat deficient in the PC-3M-luc-C6 cells.

In vitro and biochemical comparisons of PARP inhibitors

In vitro assays were performed to compare PARP-trapping activity and cytotoxicity induced by niraparib, olaparib, rucaparib, and talazoparib. In a biochemical PARP-trapping assay, the EC_{50} value was 9.8 nmol/L for niraparib, 5.3 nmol/L for olaparib, and 2.4 nmol/L for rucaparib (**Fig. 1C**). The EC_{50} value for talazoparib was below the sensitivity of the assay (<2 nmol/L). The differences in PARP trapping activity displayed by niraparib, olaparib, and rucaparib are not believed to be meaningfully different from each other, based on the assay limitations. The outcome for each drug is consistent with prior studies using a similar cell-free assay (33, 34).

A proliferation assay evaluated the relative sensitivity of the PC-3M-luc-C6 cells to the PARP inhibitors (**Fig. 1D**). Talazoparib was the most potent molecule (IC_{50} = 0.016 μmol/L), followed by niraparib, rucaparib, and olaparib (IC_{50} values of 0.11, 0.55, and 1.1 μmol/L, respectively). IC_{50} values of niraparib and talazoparib were each significantly different from every other PARP inhibitor tested ($P \leq 0.0002$); IC_{50} values for rucaparib and olaparib were not significantly different from each other. Similar proliferation assays were performed testing the 4 PARP inhibitors in DU145, LNCaP, and LNCaP-AR cells, including IC_{30}, IC_{50}, and IC_{80} values for comparison (Supplementary Table S2). Results of these assays confirmed that the PC-3M-luc-C6 cells were more sensitive to PARP inhibition than the other cell lines, and yielded a similar order of drug potency.

Steady-state PK study

The MTD of each PARP inhibitor was determined for male athymic nude mice, using published regimens as a guide (20, 26, 27). On the basis of the tolerability studies, the following dosing regimens were used: niraparib was dosed at 50 mg/kg, olaparib at 75 mg/kg, rucaparib at 150 mg/kg, and talazoparib at 0.165 mg/kg. All drugs were dosed orally once a day except for rucaparib, which was dosed twice a day.

To compare the tissue exposure profiles of the four PARP inhibitors, a steady-state PK study was performed in male mice bearing PC-3M-luc-C6 subcutaneous tumors (for detailed study design, see Supplementary Fig. S1). Results of this analysis showed that niraparib was measurable for 24 hours in plasma, tumor, and prostate and for 12 hours in the brain and bone marrow (**Fig. 2**). Rucaparib could be measured in plasma, tumor, and prostate for 24 hours, but for only 6 hours in brain and bone marrow. Olaparib was detected in tumor for 24 hours, in plasma and prostate for 12 hours, and in brain and bone marrow for 2 hours. Talazoparib was measurable in plasma and tumor for 24 hours, in prostate for 12 hours, and was undetectable at any time in brain or bone marrow. The AUC_{0-24} values (**Fig. 2**; Supplementary Table S3) and AUC_{0-24} tissue:plasma ratios (**Table 1**) summarize the steady-state PK. All the PARP inhibitors showed favorable tumor:plasma exposure ratios of greater than 1. Of the four agents, olaparib consistently showed the lowest tissue:plasma exposure ratios. Niraparib showed either comparable or superior tissue exposure for all tissues tested, particularly for bone marrow and brain, when compared with olaparib, rucaparib, and talazoparib.

Efficacy of PARP inhibitors in PC-3M-luc-C6 subcutaneous and bone metastasis tumor models

The distinct tissue:plasma exposure ratios observed in the steady-state PK study suggested that the PARP inhibitors might

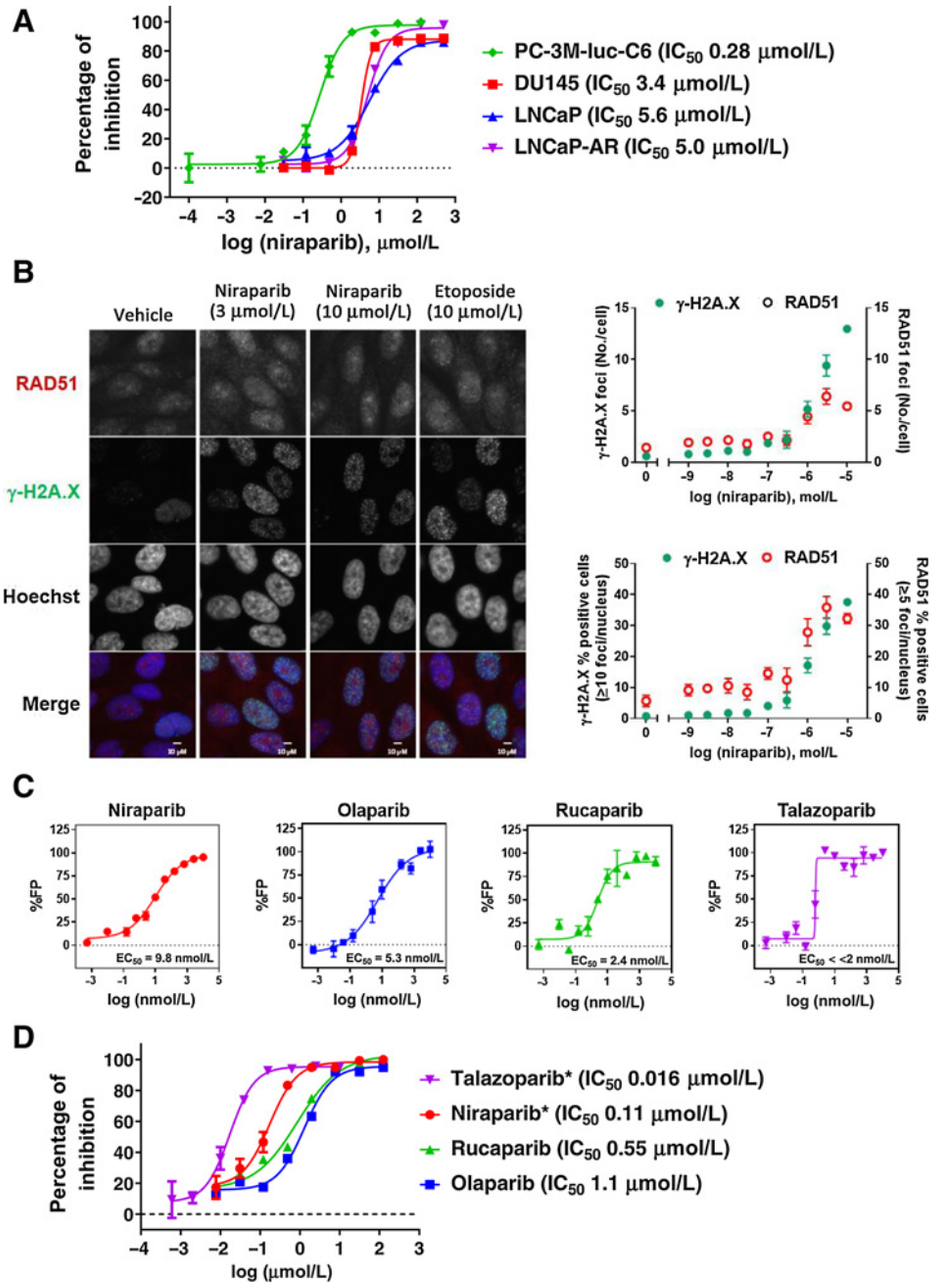

Figure 1.

Effect of PARP inhibitors on cell proliferation, DNA damage repair, and PARP trapping. **A,** Prostate tumor cell lines were treated with a concentration range of niraparib for 6 days, followed by assessment of proliferation and determination of IC_{50} values. Means ± SEM are graphed from triplicate test conditions. Representative results are shown from one of two experiments. **B,** PC-3M-luc-C6 cells were treated with vehicle, etoposide (positive control), or a concentration range of niraparib for 18 hours, followed by staining for RAD51 and γ-H2A.X, and with Hoechst dye. Representative immunofluorescent staining is shown. The graphs depict enumeration of γ-H2A.X and RAD51 foci, displayed as the number of foci/cell (top right) and the percentage of foci-positive cells (bottom right); data are graphed as the mean ± SD. **C,** PARP inhibitors were evaluated in a biochemical PARP trapping assay. Data are graphed as the percentage of fluorescence polarization, which increases as drug binds to the substrate, and graphed as means ± SEM. **D,** PC-3M-luc-C6 cells were treated with a concentration range of each PARP inhibitor for 6 days, followed by assessment of proliferation and determination of IC_{50} values. Means ± SEM are graphed from triplicate test conditions. Representative results are shown from one of two experiments. *IC_{50} value was significantly different ($P \leq 0.0002$) compared with each of the other PARP inhibitors tested in the experiment.

be differentiated by efficacy, depending on the tumor model setting. In the PC-3M-luc-C6 subcutaneous tumor model, niraparib, olaparib, and talazoparib significantly inhibited tumor growth to a similar level [38%–43% TGI on day 23; 95% CI are (36–51, 30–46, and 32–48), respectively; **Fig. 3A**, **Table 2**] when compared with the vehicle control group. Rucaparib was less effective (28% TGI; 95% CI, 21–33) than the other PARP inhibitors, although still significant compared with the vehicle control. The rate of tumor growth was significantly lower for all PARP inhibitors compared with vehicle control (**Table 2**; all P values <0.05). Rucaparib treatment resulted in a significantly higher tumor growth rate compared with niraparib treatment ($P = 0.0108$). Survival analysis showed that niraparib, olaparib, and talazoparib treatments were different from the vehicle control, by ≥25% based on ILS (**Fig. 3B**, **Table 2**). Niraparib, olaparib, and talazoparib exhibited significantly lower hazard rates, and therefore longer survival when compared with vehicle control (all P values <0.05); however, olaparib and talazoparib were not significantly different in terms of their hazard rates when compared to the niraparib group (all P values >0.05; **Table 2**). These results are consistent with the subcutaneous tumor:plasma exposure results for each PARP inhibitor, which showed tumor:plasma exposure ratios >1 for each PARP inhibitor (**Table 1**).

In contrast, results for the bone metastasis model showed that the PARP inhibitors differed in the efficacy induced by each molecule. On day 17, after 15 days of treatment, niraparib significantly inhibited tumor growth in bone compared with the control group, inducing

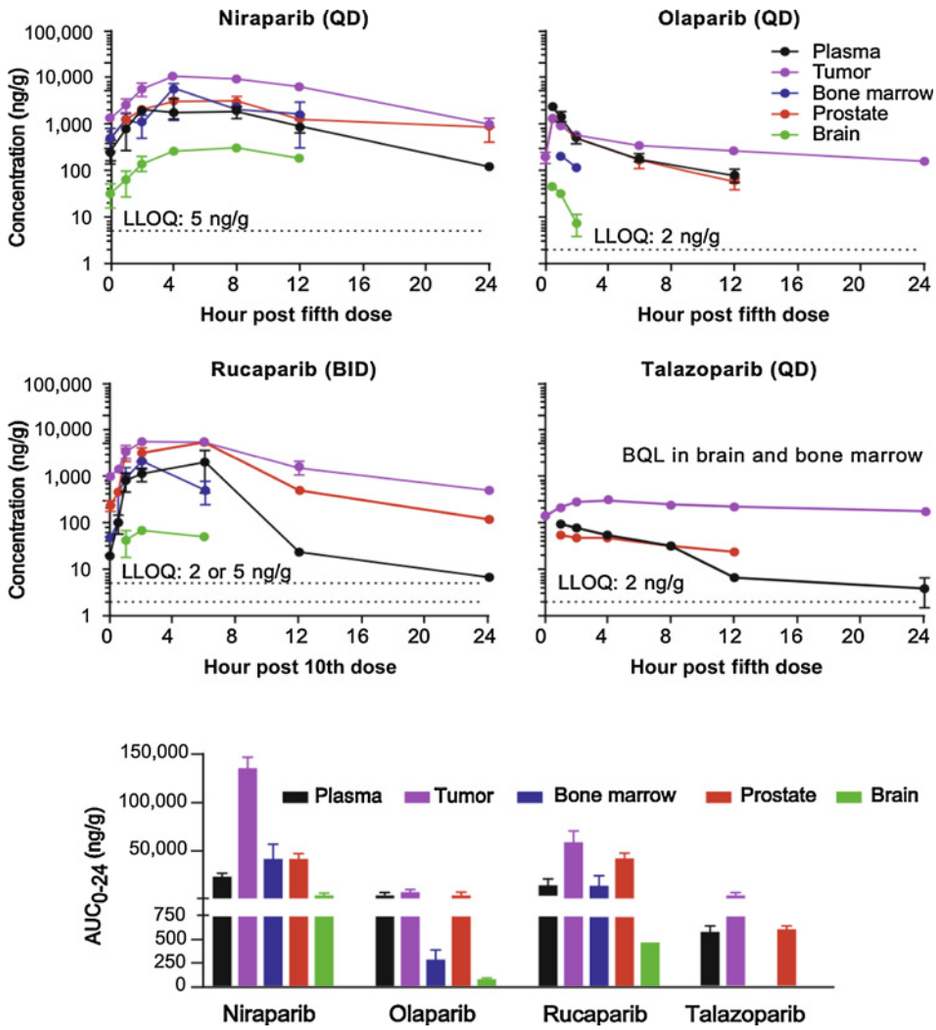

Figure 2.

Tissue distribution and exposure of PARP inhibitors from a steady-state PK study conducted in mice bearing PC-3M-luc-C6 subcutaneous tumors. QD, dosed once a day; BID, dosed twice a day; AUC_{0-24}, area under the concentration-time curve for 24 hours; BQL, below quantitation limit; LLOQ, lower limit of quantitation. Each PARP inhibitor was dosed orally at its MTD for 5 days in male mice bearing established PC-3M-luc-C6 subcutaneous tumors. Samples (n = 3/timepoint) from the indicated tissues were obtained just before the fifth dose (niraparib, olaparib, and talazoparib) or 10th dose (rucaparib), followed by sampling over the following 24 hours. Drug concentrations were determined by LC-MS/MS. The top four graphs show the concentration of each drug in tissues, graphed as the mean ± SEM; note that the y-axes are in the same log scale to enable direct comparison of the drugs. The LLOQ is indicated for each drug; the LLOQ for rucaparib varied slightly when analyses were run. The bottom bar graph compares AUC_{0-24} values for the PARP inhibitors, graphed as mean ± SEM. The top y-axis range starts at 750 ng/g. Talazoparib values could not be graphed for brain or bone marrow due to lack of detection in these tissues. Plasma samples are graphed as ng/mL.

67% TGI ($P = 0.002$; 95% CI, 44–80), followed by olaparib with 45% TGI ($P = 0.035$; 95% CI, 6–69), and 40% to 43% TGI induced by rucaparib and talazoparib ($P > 0.05$; **Fig. 3C** and **Table 3**). In addition, the rate of change of tumor growth over time differed for each PARP inhibitor. Niraparib, rucaparib, and talazoparib each induced significantly lower rates of change of BLI over time compared with the control group (all P values <0.01), whereas olaparib was not different from the control group ($P = 0.4040$; see **Table 3**). The BLI rate of change induced by niraparib was also significantly lower than the other treatment groups ($P < 0.01$ for all comparisons; **Table 3**), consistent with the greater inhibition of tumor growth observed with niraparib.

Finally, survival analysis of the bone metastasis model showed that, although all the treatments exhibited significantly lower hazard rates compared with the control group (all P values <0.05), niraparib provided the greatest benefit of the four PARP inhibitors, conferring a hazard ratio (HR) = 0.28 (**Fig. 3D**, **Table 3**). The other PARP inhibitors had higher HRs (0.46–0.59). When compared with niraparib, the other PARP inhibitors exhibited significant increases in HR (HR, 1.68–2.16, all P values <0.05; **Table 3**), confirming that niraparib provided superior survival benefit over the other agents.

Table 1. Tissue:plasma AUC_{0-24} ratios for PARP inhibitors derived from mice bearing PC-3M-luc-C6 subcutaneous tumors.

PARP Inhibitor	Tumor	Bone marrow	Prostate	Brain
Niraparib	5.7 (0.82)	1.7 (0.74)	1.7 (0.29)	0.16 (0.02)
Olaparib	1.6 (0.16)	0.06[a]	0.78 (0.11)	0.01[a]
Rucaparib	4.3 (2.6)	1.1[a]	3.2 (1.84)	0.03[a]
Talazoparib	9.3 (0.89)	NC	1.0 (0.12)	NC

Note: Means are shown with standard errors in parentheses. NC, not calculable due to lack of exposure in the tissue.
[a]Standard errors could not be calculated because of sparse data.

Discussion

PARP inhibitors comprise an important drug class that offers significant clinical benefit to patients whose tumors have defects in DDR. These molecules can be distinguished *in vitro* by their ability to inhibit PARP enzymatic activity, to induce PARP trapping, and their selectivity for members of the PARP/tankyrase family (33–35). There have been few head-to-head studies comparing tissue exposure and therapeutic activity of PARP inhibitors *in vivo* (19, 20). Such

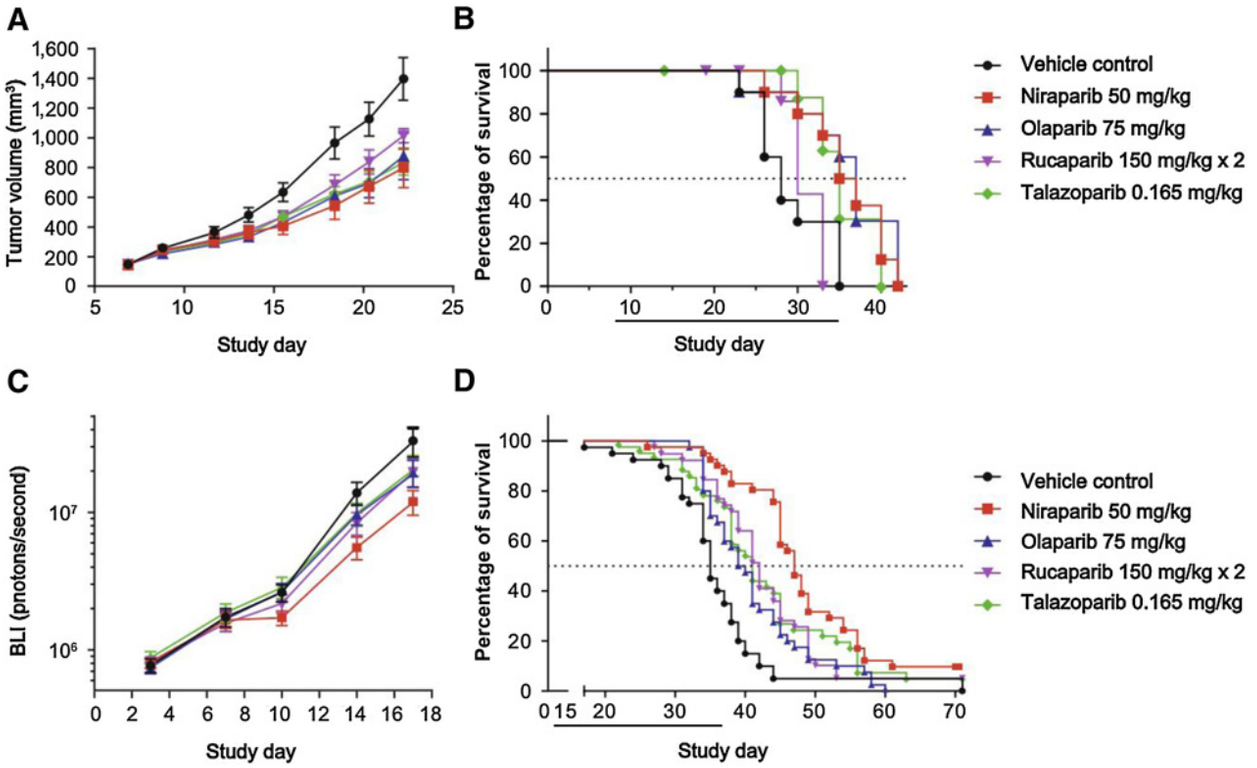

Figure 3.

Efficacy of PARP inhibitors in PC-3M-luc-C6 subcutaneous and bone metastasis models. In all *in vivo* studies, niraparib, olaparib, and talazoparib were dosed orally once a day, whereas rucaparib was dosed orally twice a day, at the indicated doses. **A** and **B,** Mice were implanted subcutaneously with PC-3M-luc-C6 tumor cells on day 0 and were randomized into groups of 10 mice, each with a mean starting tumor volume of approximately 140 mm^3. Mice were dosed from days 7 to 34 (dosing period is denoted by horizontal line below the *x*-axis in **B**). Group tumor volumes are graphed as the mean ± SEM (**A**); mice were removed from the study when individual tumor volume reached 2,000 mm^3 or adverse clinical signs were observed, and survival curves were generated (**B**). **C** and **D,** Mice were implanted with PC-3M-luc-C6 tumor cells by intracardiac injection on day 0, randomized into groups on day 3 based on body weight, and dosed with vehicle or PARP inhibitors on days 3 to 37 (dosing period is denoted by horizontal line below the *x*-axis in **D**). Results from three studies were pooled and graphed (n = 39–41/group). Bioluminescence intensity of tumors was measured from the femurs and mandible of each mouse, and graphed in log scale as the group mean ± SEM (**C**). Mice were removed from the study when body weight loss of ≥20% or adverse clinical signs were observed; survival curves were generated from these data (**D**). The horizontal dashed line in each survival graph is set at median survival of 50%.

comparisons are needed to better understand the strengths and limitations of these inhibitors and how they are best deployed for patient care, specifically in the context of prostate cancer treatment. Here, we report the first studies comparing the tissue exposures and antitumor activity of niraparib, olaparib, rucaparib, and talazoparib in subcutaneous and bone metastasis models of prostate cancer.

The paucity of human and mouse prostate tumor models that are *BRCA1* or *BRCA2* homozygous mutant and that can be studied both *in vitro* and *in vivo* presented challenges to testing our hypotheses. Although niraparib was cytotoxic toward prostate tumor lines *in vitro*, it was typically with micromolar IC_{50} values (**Fig. 1A**), rather than the low nanomolar IC_{50} values exhibited by *BRCA1* and *BRCA2* homozygous mutant tumor models (36). Bearing a monoallelic *BRCA2* mutation was insufficient to render cells sensitive to PARP inhibition, as seen with the LNCaP-AR cells *in vitro* (**Fig. 1A**; Supplementary Table S1) and *in vivo* (Supplementary Fig. S2; ref. 37). We found that tumor models with micromolar IC_{50} values *in vitro* were unaffected by PARP inhibition *in vivo* (37), confirming that *in vitro* results predicted *in vivo* outcomes. It was fortuitous that PC-3M-luc-C6 cells (lacking *BRCA1/2* homozygous mutations) exhibited submicromolar sensitivity to niraparib *in vitro;* the γ-H2A.X and RAD51 staining results further supported a defect in DDR in these cells. The PC-3M-luc-C6 model was especially useful because it can grow subcutaneously, and by ICI, it reliably seeds and grows in bone, mimicking bone metastasis. The ICI tumor injection route allows one to test whether drugs can access tumor growing in intact bone, rather than implanting tumors in bone using a bone injection method that would compromise bone integrity.

The PK study results from the PC-3M-luc-C6 subcutaneous model showed that, when dosed at their MTD, all four PARP inhibitors had sustained tumor exposure over 24 hours and had tumor:plasma AUC_{0-24} ratios greater than 1 (**Fig. 2**; **Table 1**). This correlated well with their similar efficacy in the subcutaneous tumor model. In contrast, niraparib showed a significant benefit over the other agents when measuring bone tumor growth inhibition in the PC-3M-luc-C6 bone metastasis model (**Fig. 3**; **Table 3**). This result is consistent with the observations that niraparib had the longest bone marrow exposure (12 hours) and the highest bone marrow:plasma AUC_{0-24} ratio (1.7). Olaparib and rucaparib showed briefer exposures (2 and 6 hours, respectively) and concomitantly lower bone marrow:plasma AUC_{0-24} ratios (0.06 and 1.1). Talazoparib could not be detected in bone marrow at any time, although it may have been present at levels below

Table 2. Effect of PARP inhibitor treatment on tumor growth and survival in mice bearing PC-3M-luc-C6 subcutaneous tumors.

	Day 23 vs. vehicle			TV Rate of change difference		TV Rate of change difference, 95% CI		TV Rate of change difference, *P* value	
Treatment	TGI (%)	TGI (%) 95% CI	TGI (%) *P* value	vs. vehicle	vs. niraparib	vs. vehicle	vs. niraparib	vs. vehicle	vs. niraparib
Vehicle	NA	NA	NA	NA	0.0195	NA	0.0122–0.0268	NA	<0.0001
Niraparib	43	36–51	<0.0001	−0.0195	NA	−0.0268 to −0.0122	NA	<0.0001	NA
Olaparib	38	30–46	<0.0001	−0.0147	0.0048	−0.0220 to −0.0074	−0.0025–0.0120	0.0001	0.1999
Rucaparib	28	21–33	<0.0001	−0.0097	0.0097	−0.0172 to −0.0023	0.0023–0.0172	0.0108	0.0108
Talazoparib	41	32–48	<0.0001	−0.0148	0.0046	−0.0222 to −0.0074	−0.0028–0.0120	0.0001	0.2179

	Cox PH model, hazard ratio		Cox PH model, 95% CI		Cox PH model, *P* value			
Treatment	vs. vehicle	vs. niraparib	vs. vehicle	vs. niraparib	vs. vehicle	vs. niraparib	Median lifespan days	%ILS vs. vehicle
Vehicle	NA	5.0237	NA	1.8651–13.5318	NA	0.0014	28	NA
Niraparib	0.1991	NA	0.0739–0.5362	NA	0.0014	NA	36	29
Olaparib	0.1575	0.7911	0.0555–0.4472	0.3023–2.0705	0.0005	0.6332	37	32
Rucaparib	1.0307	5.1782	0.3764–2.8226	1.6701–16.0548	0.9530	0.0044	30	7
Talazoparib	0.2738	1.3753	0.0994–0.7538	0.5024–3.7643	0.0122	0.5351	35	25

Abbreviations: CI, confidence interval; ILS, increased lifespan; NA, not applicable; PH, proportional hazards; TGI, tumor growth inhibition; TV, tumor volume.

the lower limit of quantitation. These differences in bone marrow exposure between niraparib and the other agents provide a rationale for the significant differences in tumor growth inhibition induced by niraparib in the bone metastasis model.

The PC-3M-luc-C6 bone metastasis model is complex. Tumor cells can be detected by bioluminescent imaging of the femur and mandible a few days after ICI, and tumor growth in bone was measured specifically to compare the efficacy of the PARP inhibitors at this tissue site. The PC-3M-luc-C6 model is osteolytic in nature (as opposed to the predominantly osteoblastic pattern observed in patients), causing the breakdown of bone as it grows (38). Osteolytic tumor growth would eventually allow the bone marrow to be exposed to drug as the experiment progresses and may account for the modest efficacy observed with talazoparib and olaparib, despite their lack of bone marrow exposure from the PK study. In addition, PC-3M-luc-C6 tumors arise in soft tissue sites, including lungs and lymph nodes, contributing to the tumor burden and body weight loss that led to euthanasia of mice on study. It is not known whether any of the PARP inhibitors were more effective to treat soft tissue tumors at these sites, but the favorable tissue exposure exhibited by niraparib in subcutaneous tumor and prostate compared well with the exposures exhibited by the other three agents for these tissues. Thus, we surmise that niraparib was best capable to prolong survival of the mice by more effective control of tumor growth throughout the animal. These results suggest that patients with metastatic prostate cancer may derive the most benefit from niraparib treatment because of its superior ability to

Table 3. Effect of PARP inhibitor treatment on tumor growth and survival in mice bearing PC-3M-luc-C6 bone metastases.

	Day 17 vs. vehicle			BLI rate of change difference		BLI rate of change difference, 95% CI		BLI rate of change difference, *P* value	
Treatment	TGI (%)	TGI (%) 95% CI	TGI (%) *P* value	vs. vehicle	vs. niraparib	vs. vehicle	vs. niraparib	vs. vehicle	vs. niraparib
Vehicle	NA	NA	NA	NA	0.0363	NA	0.0242–0.0485	NA	<0.0001
Niraparib	67	44–80	0.001	−0.0363	NA	−0.0485 to −0.0242	NA	<0.0001	NA
Olaparib	45	6–69	0.035	−0.0052	0.0312	−0.0173–0.0070	0.0191–0.0433	0.4040	<0.0001
Rucaparib	43	−4–68	0.067	−0.0166	0.0197	−0.0288 to −0.0045	0.0076–0.0318	0.0075	0.0014
Talazoparib	40	−13–69	0.104	−0.0175	0.0188	−0.0297 to −0.0053	0.0067–0.0310	0.0050	0.0024

	Cox PH model, hazard ratio		Cox PH model, 95% CI		Cox PH model, *P* value	
Treatment	vs. vehicle	vs. niraparib	vs. vehicle	vs. niraparib	vs. vehicle	vs. niraparib
Vehicle	NA	3.63	NA	2.29–5.76	NA	<0.0001
Niraparib	0.28	NA	0.17–0.44	NA	<0.0001	NA
Olaparib	0.59	2.16	0.38–0.93	1.37–3.39	0.024	0.0009
Rucaparib	0.47	1.70	0.29–0.74	1.07–2.68	0.0012	0.024
Talazoparib	0.46	1.68	0.29–0.73	1.07–2.65	0.0009	0.025

Abbreviations: BLI, bioluminescent imaging; CI, confidence interval; NA not applicable; PH, proportional hazards; TGI, tumor growth inhibition.

penetrate and control tumor growth in bone marrow compared with other PARP inhibitors, coupled with its ability to suppress soft tissue tumor growth. In patients with ovarian and prostate cancer treated with niraparib, hematologic toxicity is sometimes observed, manifested as anemia, leukopenia, and thrombocytopenia (7, 39). This suggests that niraparib is achieving bone marrow exposure in humans and may be capable of suppressing tumor growth in bone.

Our results are consistent with and expand on studies evaluating tissue distribution and efficacy of these PARP inhibitors. The favorable bone marrow and subcutaneous tumor exposures displayed by niraparib versus olaparib in our study are similar to those observed in breast and ovarian xenograft models (20). In addition, the very low brain exposures seen for olaparib, rucaparib, and talazoparib are consistent with studies showing that these drugs were ineffective to treat intracranial tumor models and confirmed by lack of brain tissue exposure (20, 40, 41). In contrast, niraparib significantly inhibited tumor growth in an intracranial tumor model (20). These studies further demonstrated that all four PARP inhibitors are subject to efflux transporters in the brain, but niraparib has a several-fold lower net efflux ratio compared with olaparib, which may account for niraparib's superior brain exposure (20). An additional advantage for niraparib may be its higher apparent permeability coefficient (21), whereas the other compounds have low solubility in aqueous solution and moderate or low cell permeability (22–24). Thus, although these drugs are differentiated *in vitro* by cytotoxic activity and PARP trapping, our studies show that the best predictor of comparative *in vivo* efficacy was the tissue distribution observed for each drug.

A limitation of our studies was the use of immunocompromised mice, which did not allow study of tumor:immune microenvironment interaction in the presence of PARP inhibition. Studies suggest there is potential for PARP inhibitors to be combined with immunotherapies (42, 43), particularly in BRCA-deficient tumor settings. Future directions may include the study of BRCA-deficient murine prostate tumor models to better understand these interactions.

Authors' Disclosures

L.A. Snyder reports a patent for Methods of treating prostate cancer pending to Janssen Pharmaceuticals. R. Hawkins reports a patent 11,207,311 issued. No disclosures were reported by the other authors.

Authors' Contributions

L.A. Snyder: Conceptualization, data curation, formal analysis, supervision, validation, investigation, visualization, methodology, writing–original draft, writing–review and editing. **R. Damle:** Conceptualization, writing–review and editing. **S. Patel:** Supervision, investigation, writing–original draft, writing–review and editing. **J. Bohrer:** Investigation, writing–original draft, writing–review and editing. **A. Fiorella:** Investigation, writing–review and editing. **J. Driscoll:** Formal analysis, investigation, writing–review and editing. **R. Hawkins:** Formal analysis, supervision, investigation, writing–review and editing. **C.F. Stratton:** Formal analysis, investigation, writing–review and editing. **C.D. Manning:** Formal analysis, investigation, writing–review and editing. **K. Tatikola:** Formal analysis, writing–review and editing. **V. Tryputsen:** Formal analysis, methodology, writing–review and editing. **K. Packman:** Conceptualization, writing–review and editing. **R.N.V.S. Mamidi:** Conceptualization, resources, writing–review and editing.

Acknowledgments

We thank Drs. J. Wang, S. Wang, and K. Sun for helpful discussions about the steady-state PK study design. We thank Dr. J. Sendecki of Janssen Research and Development, LLC for consultation on statistical methods. We thank Drs. E. Trachet and S. Krueger of Covance for their extensive advice and guidance on the PC-3M-luc-C6 subcutaneous and ICI models. The *in vitro* DNA damage repair studies were performed by Horizon Discovery, Ltd., and the *in vivo* PK and efficacy studies were performed by Covance; both were funded by Janssen Research and Development, LLC. Writing assistance was provided by Colleen Elliott of CME Science Writers and funded by Janssen Research and Development, LLC. Graphic support was provided by SIRO Clinpharm Pvt. Ltd. and funded by Janssen Global Services, LLC.

The costs of publication of this article were defrayed in part by the payment of page charges. This article must therefore be hereby marked *advertisement* in accordance with 18 U.S.C. Section 1734 solely to indicate this fact.

Received September 26, 2021; revised February 14, 2022; accepted April 19, 2022; published first May 2, 2022.

References

1. Siegel RL, Miller KD, Jemal A. Cancer statistics, 2020. CA Cancer J Clin 2020;70:7–30.
2. Velho PI, Bastos DA, Antonarakis ES. New approaches to targeting the androgen receptor pathway in prostate cancer. Clin Adv Hematol Oncol 2021;19:228–40.
3. Robinson D, Van Allen EM, Wu YM, Schultz N, Lonigro RJ, Mosquera JM, et al. Integrative clinical genomics of advanced prostate cancer. Cell 2015;162:454.
4. Farmer H, McCabe N, Lord CJ, Tutt AN, Johnson DA, Richardson TB, et al. Targeting the DNA repair defect in BRCA mutant cells as a therapeutic strategy. Nature 2005;434:917–21.
5. Pommier Y, O'Connor MJ, de Bono J. Laying a trap to kill cancer cells: PARP inhibitors and their mechanisms of action. Sci Transl Med 2016;8:362ps17.
6. Ledermann J, Harter P, Gourley C, Friedlander M, Vergote I, Rustin G, et al. Olaparib maintenance therapy in patients with platinum-sensitive relapsed serous ovarian cancer: a preplanned retrospective analysis of outcomes by BRCA status in a randomised phase 2 trial. Lancet Oncol 2014;15:852–61.
7. Mirza MR, Monk BJ, Herrstedt J, Oza AM, Mahner S, Redondo A, et al. Niraparib maintenance therapy in platinum-sensitive, recurrent ovarian cancer. N Engl J Med 2016;375:2154–64.
8. Swisher EM, Lin KK, Oza AM, Scott CL, Giordano H, Sun J, et al. Rucaparib in relapsed, platinum-sensitive high-grade ovarian carcinoma (ARIEL2 Part 1): an international, multicentre, open-label, phase 2 trial. Lancet Oncol 2017;18:75–87.
9. Konstantinopoulos PA, Ceccaldi R, Shapiro GI, D'Andrea AD. Homologous recombination deficiency: exploiting the fundamental vulnerability of ovarian cancer. Cancer Discov 2015;5:1137–54.
10. Abida W, Patnaik A, Campbell D, Shapiro J, Bryce AH, McDermott R, et al. Rucaparib in men with metastatic castration-resistant prostate cancer harboring a BRCA1 or BRCA2 gene alteration. J Clin Oncol 2020;38:3763–72.
11. de Bono J, Mateo J, Fizazi K, Saad F, Shore N, Sandhu S, et al. Olaparib for metastatic castration-resistant prostate cancer. N Engl J Med 2020;382:2091–102.
12. Mateo J, Carreira S, Sandhu S, Miranda S, Mossop H, Perez-Lopez R, et al. DNA-repair defects and olaparib in metastatic prostate cancer. N Engl J Med 2015;373:1697–708.
13. Smith MR, Sandhu SK, Kelly WK, Scher HI, Efstathiou E, Lara P, et al. Phase II study of niraparib in patients with metastatic castration-resistant prostate cancer (mCRPC) and biallelic DNA-repair gene defects (DRD): preliminary results of GALAHAD. J Clin Oncol 2019;37:202.
14. Smith MR, Sandhu SK, Kelly WK, Scher HI, Efstathiou E, Lara PN, et al. Pre-specified interim analysis of GALAHAD: a phase 2 study of niraparib in patients (pts) with metastatic castration-resistant prostate cancer (mCRPC) and biallelic DNA-repair gene defects (DRD). Ann Oncol 2019;30:V884–5.
15. Patrikidou A, Brureau L, Casenave J, Albiges L, Di Palma M, Patard JJ, et al. Locoregional symptoms in patients with *de novo* metastatic prostate cancer: morbidity, management, and disease outcome. Urol Oncol 2015;33:202.e9–17.
16. Lin SR, Mokgautsi N, Liu YN. Ras and Wnt interaction contribute in prostate cancer bone metastasis. Molecules 2020;25:2380.
17. Nieder C, Haukland E, Pawinski A, Dalhaug A. Anaemia and thrombocytopenia in patients with prostate cancer and bone metastases. BMC Cancer 2010;10:284.

18. Quiroz-Munoz M, Izadmehr S, Arumugam D, Wong B, Kirschenbaum A, Levine AC. Mechanisms of osteoblastic bone metastasis in prostate cancer: role of prostatic acid phosphatase. J Endocr Soc 2019;3:655–64.
19. Leo E, Johannes J, Illuzzi G, Zhang A, Hemsley P, Bista MJ, et al. A head-to-head comparison of the properties of five clinical PARP inhibitors identifies new insights that can explain both the observed clinical efficacy and safety profiles. AACR Annual Meeting; April 14–18, 2018. Clin Cancer Res 2018;78(13 suppl). Abstract LB-273. doi:10.1158/1538-7445.AM2018-LB-273.
20. Sun K, Mikule K, Wang Z, Poon G, Vaidyanathan A, Smith G, et al. A comparative pharmacokinetic study of PARP inhibitors demonstrates favorable properties for niraparib efficacy in preclinical tumor models. Oncotarget 2018;9:37080–96.
21. European Medicines Agency Assessment Report for EMA/648982/2017. Published September 2017. Accessed June 4, 2022. https://www.ema.europa.eu/en/documents/assessment-report/zejula-epar-public-assessment-report_en.pdf.
22. Center for Drug Evaluation and Research. Clinical Pharmacology Filing Form for New Drug Approval. 206162. Published February 2014. Accessed June 4, 2022. https://www.accessdata.fda.gov/drugsatfda_docs/nda/2014/206162Orig1s000Approv.pdf.
23. Center for Drug Evaluation and Research. Multi-disciplinary Review and Evaluation NDA 211651. Published April 2018. Accessed June 4, 2022. https://www.accessdata.fda.gov/drugsatfda_docs/nda/2018/211651Orig1s000MultidisciplineR.pdf.
24. European Medicines Agency. Science Medicine Health Assessment Report for EMA/CHMP/238139/2018. Published March 2018. Accessed June 4, 2022. https://www.ema.europa.eu/en/documents/assessment-report/rubraca-epar-public-assessment-report_en.pdf.
25. Chen CD, Welsbie DS, Tran C, Baek SH, Chen R, Vessella R, et al. Molecular determinants of resistance to antiandrogen therapy. Nat Med 2004;10:33–9.
26. Shen Y, Rehman FL, Feng Y, Boshuizen J, Bajrami I, Elliott R, et al. BMN 673, a novel and highly potent PARP1/2 inhibitor for the treatment of human cancers with DNA repair deficiency. Clin Cancer Res 2013;19:5003–15.
27. Robillard L, Nguyen M, Loehr A, Orsulic S, Kristeleit R, Lin K, et al. Preclinical evaluation of the PARP inhibitor rucaparib in combination with PD-1 and PD-L1 inhibition in a syngeneic BRCA1 mutant ovarian cancer model [abstract]. In: Proceedings of AACR Annual Meeting; April 1–5, 2017. Clin Cancer Res 2017;77(13 suppl):3650. Abstract 36502017.
28. Yeh C. Estimation and significant tests of area under the curve derived from incomplete blood sampling. In: American Statistical Association Proceedings of the Biopharmaceutical Section. American Statistical Association; 1990. p. 74–81.
29. Holder DJ, Hsuan F, Dixit R, Soper K. A method for estimating and testing area under the curve in serial sacrifice, batch, and complete data designs. J Biopharm Stat 1999;9:451–64.
30. Jaki TWM. A theoretical framework for estimation of AUCs in complete and incomplete sampling designs. Stat Biopharm Res 2009;1:176–84.
31. Bonner WM, Redon CE, Dickey JS, Nakamura AJ, Sedelnikova OA, Solier S, et al. GammaH2AX and cancer. Nat Rev Cancer 2008;8:957–67.
32. Paull TT, Rogakou EP, Yamazaki V, Kirchgessner CU, Gellert M, Bonner WM. A critical role for histone H2AX in recruitment of repair factors to nuclear foci after DNA damage. Curr Biol 2000;10:886–95.
33. Murai J, Huang SY, Das BB, Renaud A, Zhang Y, Doroshow JH, et al. Trapping of PARP1 and PARP2 by clinical PARP inhibitors. Cancer Res 2012;72:5588–99.
34. Murai J, Huang SY, Renaud A, Zhang Y, Ji J, Takeda S, et al. Stereospecific PARP trapping by BMN 673 and comparison with olaparib and rucaparib. Mol Cancer Ther 2014;13:433–43.
35. Thorsell AG, Ekblad T, Karlberg T, Low M, Pinto AF, Tresaugues L, et al. Structural basis for potency and promiscuity in Poly(ADP-ribose) polymerase (PARP) and tankyrase inhibitors. J Med Chem 2017;60:1262–71.
36. Jones P, Altamura S, Boueres J, Ferrigno F, Fonsi M, Giomini C, et al. Discovery of 2-{4-[(3S)-piperidin-3-yl]phenyl}-2H-indazole-7-carboxamide (MK-4827): a novel oral poly(ADP-ribose)polymerase (PARP) inhibitor efficacious in BRCA-1 and -2 mutant tumors. J Med Chem 2009;52:7170–85.
37. Damle RN, Hawkins R, Hosbach J, Habineza Ndikuyeze G, Driscoll J, Fulton N, et al. Niraparib combined with abiraterone acetate inhibits the growth of BRCA2wt prostate tumors. Cancer Res 2019;79;2134.
38. Cross NA, Fowles A, Reeves K, Jokonya N, Linton K, Holen I, et al. Imaging the effects of castration on bone turnover and hormone-independent prostate cancer colonization of bone. Prostate 2008;68:1707–14.
39. Gonzalez-Martin A, Pothuri B, Vergote I, DePont Christensen R, Graybill W, Mirza MR, et al. Niraparib in patients with newly diagnosed advanced ovarian cancer. N Engl J Med 2019;381:2391–402.
40. Kizilbash SH, Gupta SK, Chang K, Kawashima R, Parrish KE, Carlson BL, et al. Restricted delivery of talazoparib across the blood–brain barrier limits the sensitizing effects of PARP inhibition on temozolomide therapy in glioblastoma. Mol Cancer Ther 2017;16:2735–46.
41. Parrish KE, Cen L, Murray J, Calligaris D, Kizilbash S, Mittapalli RK, et al. Efficacy of PARP inhibitor rucaparib in orthotopic glioblastoma xenografts is limited by ineffective drug penetration into the central nervous system. Mol Cancer Ther 2015;14:2735–43.
42. Pantelidou C, Sonzogni O, De Oliveria Taveira M, Mehta AK, Kothari A, Wang D, et al. PARP inhibitor efficacy depends on CD8(+) T-cell recruitment via intratumoral STING pathway activation in BRCA-deficient models of triple-negative breast cancer. Cancer Discov 2019;9:722–37.
43. Reislander T, Lombardi EP, Groelly FJ, Miar A, Porru M, Di Vito S, et al. BRCA2 abrogation triggers innate immune responses potentiated by treatment with PARP inhibitors. Nat Commun 2019;10:3143.